Chemical Engineering Journal 401 (2020) 126111

Contents lists available at ScienceDirect

Chemical Engineering Journal

journal homepage: www.elsevier.com/locate/cej

Low energy consumption and mechanism study of redox flow desalination

Fuming Chen[a,*], Jian Wang[a], Chunhua Feng[b], Jinxing Ma[c], T. David Waite[c]

[a] Guangdong Provincial Key Laboratory of Quantum Engineering and Quantum Materials, Guangdong Engineering Technology Research Center of Efficient Green Energy and Environment Protection Materials, School of Physics and Telecommunication Engineering, South China Normal University, Guangzhou 510006, PR China
[b] School of Environment and Energy, South China University of Technology, Guangzhou 510006, PR China
[c] UNSW Water Research Centre, School of Civil and Environmental Engineering, University of New South Wales, Sydney, New South Wales 2052, Australia

HIGHLIGHTS

- Less than 150 ppm water product can be obtained by one-time-continuous charge process in batch mode.
- The removal efficiency is up to 95.5% for single-continuous batch-mode treatment.
- An unlimited salt removal capacity was demonstrated.
- A relatively low average energy consumption down to 8.34 kJ mole^{-1} salt removed is achievable.
- No electrode regeneration is required to realize the full continuous desalination.

GRAPHICAL ABSTRACT

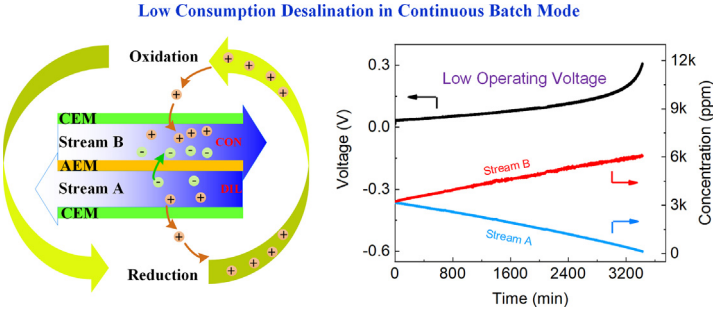

ARTICLE INFO

Keywords:
Electrochemical desalination
Energy consumption
Redox couples
Water purification

ABSTRACT

Low-energy desalination technologies capable of continuous throughput at reasonable operating and maintenance cost are now critically needed. Herein, we present a continuous desalination process with average energy consumption as low as 2.14 kJ mole^{-1} salt removed achievable when using a 10 mM/10 mM ferri-/ferrocyanide solution that flows continuously between anode and cathode chambers. The salt feed at ~3000 ppm can be continuously desalted to a potable level of less than 150 ppm during the desalination process. At the anode, ferrocyanide is oxidized with electrons released to the external circuit and cations captured to achieve charge balance. Ferricyanide is reduced at the cathode, resulting in the constant transfer of anions from the dilute stream to the concentrate stream. The recycling of the redox mediators maintains an extremely low operating potential (~100 mV) and continuous salt extraction with unlimited removal capacity. Comparison of the use of ferri-/ferrocyanide, pure ferricyanide and ferrocyanide solutions indicate that the ultra-low energy consumption can be ascribed to the excellent electrochemical properties of the ferri-/ferrocyanide couple and the extremely low overpotential of the redox reactions owing to the synergistic effect of sufficient simultaneous ferrocyanide oxidation and ferricyanide reduction in the flow electrolyte streams. Our research provides a route for ultra-low energy desalination based on voltage suppression via use of facile redox couple mediators.

1. Introduction

Both low energy consumption and the capability of continuous desalination are critical issues in view of the need for freshwater production from seawater and brackish water. While commercial desalination technologies such as reverse osmosis (RO), thermal distillation

* Corresponding author.
E-mail addresses: fmchen@scnu.edu.cn (F. Chen), chfeng@scut.edu.cn (C. Feng), jinxing.ma@unsw.edu.au (J. Ma), d.waite@unsw.edu.au (T. David Waite).

https://doi.org/10.1016/j.cej.2020.126111
Received 22 March 2020; Received in revised form 25 June 2020; Accepted 26 June 2020
Available online 02 July 2020

and electrodialysis that can potentially achieve these targets have been applied at industrial scale, both the capital investments and operating costs (e.g. ranging from 0.5 to 2.5 kWh m^{-3} for brackish water to 3–10 kWh m^{-3} for seawater with specific energy cost of 40–60 kJ per mole salt removed) [1] are very high. Alternatively, capacitive deionization (CDI) has been proposed as an "energy-saving" desalination technology [2,3]. In conventional CDI, salt removal is associated with the sorption of ions in the electrical double layers at the carbon electrodes and, as such, concern remains with regard to its productivity compared to the existing alternatives due to the limited ion sorption capacity of the carbon materials. Moreover, most CDI devices employ two separated electrodes which result in the necessity for intermittent desalination/salination [4–7].

In order to enhance the salt removal capacity, Faradaic electrodes have been prepared via the use of Faradaic-active materials and carbon additives [8,9]. Electron transfer as a result of the Faradaic reactions occurring on the electrodes contributes to the concomitant ion capture/storage with the periodic reversal of these reactions resulting in alternative desalination and salination. It has been reported that a dual-ion Faradaic electrochemical deionization system possesses ion capture capacity more than six times that of a traditional CDI unit [10–12]. Recent deionization designs involving the use of Faradaic-active electrodes include "rocking chair" desalination [13–15], a redox flow battery system [16,17] and other novel desalination processes [18–23] with most of these designs involving use of fluidized Faradaic-active electrodes (or use of Faradaic-active electrolytes [15,24,25]) in view of their capacity to overcome the limited specific capacity of solid electrodes [26]. Nevertheless, most of these desalination processes are not operated in continuous mode with the energy consumption up to ~100 kJ $mole^{-1}$ salt removed. For example, our latest research work demonstrated that while a metal-free organic mediator can be used for continuous desalination if the positive and negative flow electrodes were connected in series, its relatively high energy cost (78 kJ $mole^{-1}$) would likely limit its application [27]. Very recently, Kim et al. carried out an interesting investigation on use of ferri-/ferrocyanide in CDI configuration under constant voltage (1.2 V) [28]. While continuous operation was achievable via reversal of the polarity, the length of one cycle was still hindered by the salt adsorption capacity (SAC, 67.8 mg g^{-1} in the study). In addition, the salt content was constantly accumulated in the redox channel during desalination due to the single salt stream design. Owing to the intrinsic features, the redox flow desalination has also drawn the attention of experts from the industry such as PARC, A Xerox Company in the United States [29]. In this work, Beh et al. presented an energy saving method to electrochemically separate water by means of the soluble reactant 1,1′-Bis[3-(trimethylammonio)-propyl] ferrocene dichloride that is continuously circulated between electrodes at constant voltage condition (0.5 V and 0.2 V). While the pioneering design of redox flow desalination was proposed in this work, the optimization of the technique and proposed mechanism is incomplete.

In view of the issues raised above, the integration of continuous operation and low energy consumption with use of an energy-saving electrode/electrolyte could well provide a breakthrough in development of electrochemical desalination technologies. In this study, we present a continuous and ultra-low energy desalination method based on voltage suppression associated with the redox reactions of the ferri-/ferrocyanide couple. When applying a constant current (Fig. 1a), ferricyanide is reduced to ferrocyanide in the cathode chamber with cations captured from the neighboring desalination chamber through the cation exchange membrane (CEM). Meanwhile, in the anode chamber, ferrocyanide is oxidized to ferricyanide with the cations released to the neighboring concentrate chamber via the other CEM. The movement of anions through the anion exchange membrane (AEM) between the desalination and concentrate chambers ensures that electroneutrality is maintained (Fig. 1a) with this process resulting in constant desalination of the incoming brackish stream and generation of a high salinity concentrate stream. Since the electrolytes are continuously recirculated between the electrode chambers, desalination can be achieved at unlimited salt removal capacity. The as-prepared salt feed (~3 g L^{-1}) can be continuously desalinated to < 150 ppm with a relatively low average energy consumption (of 8.34 kJ $mole^{-1}$ salt removed) achievable with use of 2 mM/2 mM ferri-/ferrocyanide redox couples at an applied current density of 0.06 mA cm^{-2}. The mechanism underlying the energy saving features of this approach is investigated here with the insights gained expected to facilitate further development of this potentially useful electrochemical desalination technology.

2. Materials and methods

2.1. Materials and experimental setup

A schematic diagram of the desalination system based on the redox reactions between ferricyanide and ferrocyanide is shown in Fig. 1a. The device consists of the following parts (Fig. S1): an anode chamber (3 cm × 3 cm × 2 mm), a cathode chamber (3 cm × 3 cm × 2 mm), two salt feed chambers (A: desalination chamber and B: concentrate chamber with dimensions of 3 cm × 3 cm × 2 mm), two pieces of graphite paper (thickness 200 μm), two pieces of carbon foam (3 cm × 3 cm × ~2.5 mm, bulk density 0.05 g cm^{-3}, porosity 96.5%), two pieces of cation exchange membrane (standard grade CEM, Tokuyama, Japan) and one piece of anion exchange membrane (standard grade AEM, Tokuyama, Japan). All separating sheets were made from acrylic plates and held together by two end plates. The graphite paper and carbon foam were combined to form the current collectors. The AEM was placed between the salt feed chambers (Figs. 1a and S1) and the CEMs were placed between the cathode chamber and the desalination chamber (A) and the anode chamber and the concentrate chamber (B) respectively. The electrode chambers were connected to each other using soft tubes with the electrolytes circulated by a peristaltic pump (LEAD FLUID, BT300S, China). The salt feed in chambers A and B were recirculated independently (Fig. S1).

The anode and cathode chambers were both fed with ferri-/ferrocyanide solution with concentrations ranging from 1 mM/1 mM to 10 mM/10 mM. The electrolytes were prepared by dissolving $K_3Fe(CN)_6$ (Energy Chemical, 99%) and $K_4Fe(CN)_6{\cdot}3H_2O$ (Macklin, ≥99.5%) with a mole ratio of 1:1 in a 3000 ppm NaCl (Aldrich, 99.5%) solution (total volume of 50 mL). The desalination and concentrate chambers (A and B) were fed with two saline streams at the same concentrations (NaCl: 3000 ppm) and identical volumes (25 mL).

2.2. Characterization of the desalination performance

All desalination tests were conducted by a battery analyser (Neware, Shenzhen, China) at room temperature. The peristaltic pumps were operated at a constant flow rate of 11.6 mL min^{-1}, where a lower operating voltage but similar desalination performance was obtained (Fig. S2). The ferri-/ferrocyanide stream and salt streams were respectively fed into the electrode chambers and the desalination and concentrate chambers (A and B); that is, all tests were run in batch mode. Before desalination, the solutions were kept circulating for two hours at current density $i = 0$. Various current densities (i = 0.06–0.24 mA·cm^{-2}) were then applied to the cell to evaluate the desalination performance. The variation of salt concentrations in streams A and B were recorded by conductivity meters (EPU357, EDAQ, Australia). Note that the impact of pH excursion on conversion of measured conductivity to salt concentration was minimal in this study because all pH values of streams A and B were circumneutral. As for cation migration to the concentrate chamber, while the presence of K^+ (from $K_4Fe(CN)_6$ on oxidation to $K_3Fe(CN)_6$) might influence the conductivity slightly as a result of the 3–5% difference at the 3000 ppm concentration of these salts in the concentrate chamber (B), the effect is considered to be negligible, particularly in view of the significantly

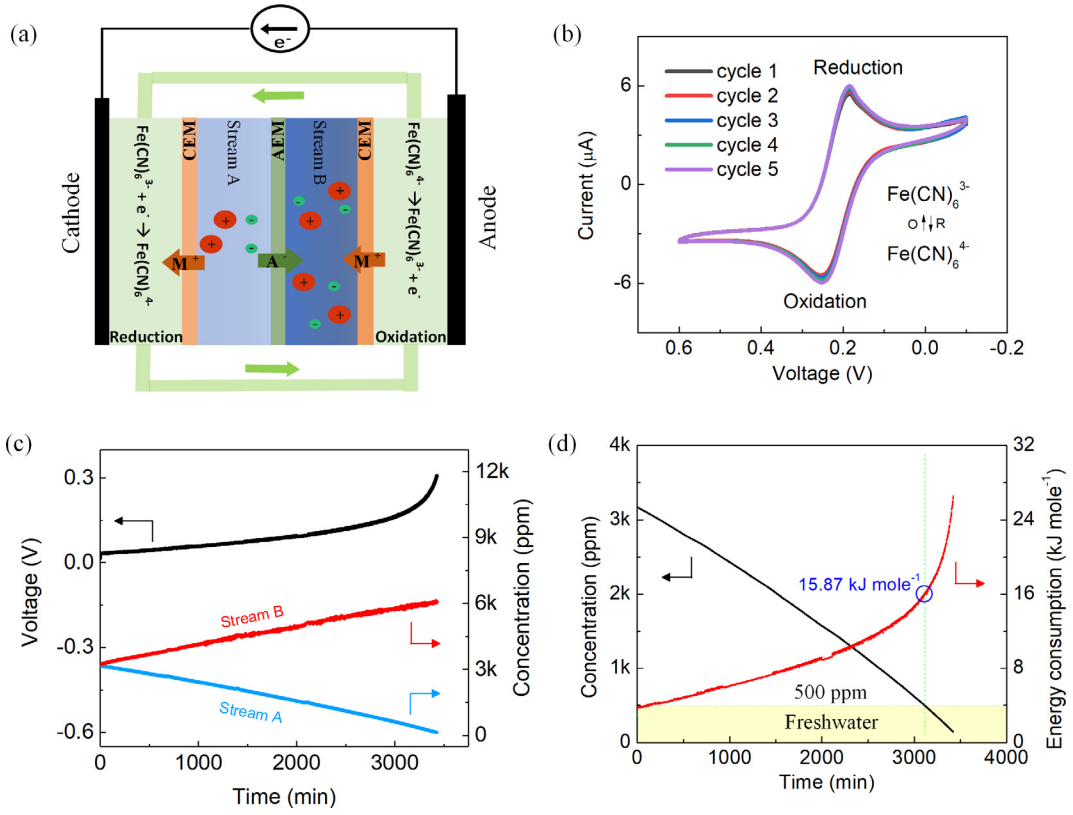

Fig. 1. (a) Schematic of the continuous desalination system with ferri-/ferrocyanide redox mediators. (b) The three-electrode CV of 2 mM/2 mM ferri-/ferrocyanide. The scanning window is from −0.1 to 0.6 V at a scanning rate of 5 mV s^{-1}. A glassy carbon electrode was used as the working electrode, a Pt grid as the counter electrode and a standard Ag/AgCl electrode as reference in the 2 mM/2 mM ferri-/ferrocyanide solution with conductivity enhancement achieved via NaCl addition. (c) Features of the continuous desalination process with 2 mM/2 mM ferri-/ferrocyanide at current density i of 0.06 mA cm^{-2}. (d) The change of salt concentration and instant energy consumption (in units of kJ $mole^{-1}$ salt removed) during the continuous desalination process.

lower concentration of salts in the desalination chamber (A).

2.3. Electrochemical measurements

The electrochemical 3-electrode cyclic voltammetry (CV) experiments were carried out in a 0.5 M NaCl electrolyte solution containing 2 mM ferricyanide and 2 mM ferrocyanide by using an electrochemical workstation (CHI760E, CH Instruments, Ins, USA). The working electrode was a glassy carbon rod (d = 3 mm) which was polished using Al_2O_3 suspended in deionized water. The Pt grid and standard Ag/AgCl electrode were used as the counter and reference electrodes, respectively. The scan rate was controlled at 5 mV·s^{-1} with the working window ranging from −0.1 to 0.6 V (*vs.* Ag/AgCl).

All linear sweep voltammetry (LSV) measurements were conducted using a Gamry RDE710 Rotating Electrode system which consisted of a glassy carbon disk working electrode (d = 5 mm), a glassy carbon counter electrode and a standard Ag/AgCl reference electrode. Before tests, nitrogen gas was used to purge the electrolyte for 30 min to remove dissolved oxygen. The electrode was rotated from 300 to 2400 rpm with an increment of 300 rpm. LSV scans were recorded at a rate of 5 mV·s^{-1}. At each rotation rate, the data were recorded three times to guarantee the repeatability. For the overpotential from 10 to 200 mV derived at zero-current potential for the reduction of ferricyanide and the oxidation of ferrocyanide, the current (i) at each rotation rate can be determined from the LSV plots with the reciprocals of current and square of rotation rate fitted linearly based on the Koutecky–Levich equation (Eq. (1)). Each Y-intercept, defined as $1/i_k$, was the reciprocal of the limiting current under the corresponding overpotential. Due to the different limiting currents for ferricyanide and ferrocyanide, the absolute limiting current ($|i_K|$) was adopted for comparison purposes. The Tafel plots of overpotential *vs.* log $|i_K|$ were then constructed for ferricyanide and ferrocyanide.

$$\frac{1}{i} = \frac{1}{i_K} + \frac{1}{0.62nFAc_0D^{2/3}\omega^{1/2}\upsilon^{-1/6}} \quad (1)$$

where n = 1 for the one electron process, Faraday's constant F = 96485 C $mole^{-1}$, electrode area A = 0.196 cm^2, c_0 is the concentration of the active electrolyte (*i.e.* ferricyanide or ferrocyanide), D is the diffusion coefficient and kinematic viscosity υ = 0.009 cm^2 s^{-1} for 0.5 M NaCl solution.

2.4. Calculation procedures

Average salt removal rate (ASRR, μg cm^{-2} min^{-1}), which describes the desalination rate, can be calculated using Eq. (2): [30,31]

$$ASRR = \frac{\left(\frac{\Delta c}{\Delta t} \times V\right)}{A_{cell}} \quad (2)$$

where $\Delta c/\Delta t$ is the salt concentration change per minute (Δppm min^{-1}), V is the volume of the salt stream (25 mL) and the cross sectional area of the cell A_{cell} is 9 cm^2.

Charge efficiency (Λ, %), defined as the percentage of salt removed to electrons used, is regarded as one of most significant parameters in characterizing desalination performance. It can be determined by the following formula:

$$\Lambda = \frac{ASRR \times F}{60 \times 10^3 \times i \times M} \quad (3)$$

where i is the current density (mA cm^{-2}) and M is the molar mass of NaCl (58.44 g $mole^{-1}$).

Energy consumption ($\bar{E}$, kJ mole^{-1}) can be calculated as follows:

$$\bar{E} = \frac{3.6\Delta E}{\left[(c_0 - c_t) \times \frac{V}{10^6 \times M}\right]} \quad (4)$$

where ΔE is the total energy consumption (Wh) during charging and c_0 and c_t are the NaCl concentrations (in ppm) initially and at time t.

3. Result and discussion

3.1. Continuous desalination with the ferri-/ferrocyanide redox couple

To investigate the redox behavior of the ferri-/ferrocyanide solution, three-electrode cyclic voltammetry was first carried out using solutions containing 2 mM of both $K_4Fe(CN)_6$ and $K_3Fe(CN)_6$. The results in Fig. 1b indicate that there is only one pair of redox peaks; the reduction peak is located at 0.19 V while the corresponding oxidation peak is at 0.25 V. At the anode, ferrocyanide can be oxidized to ferricyanide, as described by the following reaction:

$$\text{Oxidation: } Fe(CN)_6^{4-} \rightarrow Fe(CN)_6^{3-} + e^- \quad (5)$$

At the cathode, ferricyanide is reduced to ferrocyanide as follows:

$$\text{Reduction: } Fe(CN)_6^{3-} + e^- \rightarrow Fe(CN)_6^{4-} \quad (6)$$

On applying a constant current (Fig. 1c), the aqueous ferricyanide is reduced in the cathode chamber and sodium ions in stream A are transported through the CEM. Subsequently, the resultant ferrocyanide is oxidized in the anode chamber with cations released to stream B through the other CEM. At the same time, chloride ions in stream A will be transported via the middle AEM to stream B (to achieve charge balance). Overall, salts in stream A are continuously removed to stream B with the salt content in the redox-active electrolyte unchanged, as observed in Fig. 1c. The present electro-deionization system is similar to electro-dialysis [32]. Specifically, the desalination process is based on the electro-dialysis of the redox reaction of ferri-/ferrocyanide redox couples. The continuous operation can be achieved with a water recovery of 50%. Note that this parameter could be further improved by decreasing the concentrate volume. It is also noted that the operating voltage can be maintained at ~0.1 V in the constant current test with this low voltage most likely a result of the facile transfer of electrons between the ferri-/ferrocyanide redox couple. Nevertheless, there was slight rise, likely due to the negligible charge accumulation. The low voltage consequently resulted in average energy consumption as low as 8.34 kJ mole^{-1} with the final water product < 150 ppm (much lower than can be achieved by commercial RO systems (details shown in Fig. S3)). The energy consumption as a function of desalination time is displayed in Fig. 1d. It can be seen that the initial instant energy consumption ($\bar{E}$) was 2.87 kJ mole^{-1} (time = 0 min). With continuation of the desalination process, more energy is consumed, which is consistent with the voltage trend in Fig. 1c. By the time the product water achieves a NaCl content of 500 ppm (after 3120 min), the instant energy consumption has reached 15.87 kJ mole^{-1} (t = 3120 min). The average energy consumption over this time period is estimated to be on the order of 7.96 kJ mole^{-1}. The time required to achieve sufficient desalination is obviously excessive but could be decreased by increasing the active electrode surface area. For example, an increase in electrode surface area from the current 9 cm^2 to 0.9 m^2 (*i.e.* an increase by a factor of 1000) would, in principle, reduce the time for desalination to around 3 min, a much more reasonable value for a viable treatment process [33,34]. The capacity of this unit of 11.6 mL min^{-1} however is far lower than required in a full scale unit. An increase in flow rate by, say, a factor of 1000 could be achieved by arrangement of 1000 units in parallel with such an arrangement enabling salt removal from 11.52 m^3 of brackish water per day at an energy consumption of around 7.96 kJ mole^{-1} of salt removed (or 0.094 kWh m^{-3} for removal of salt from a brackish feed stream containing 3000 ppm of salt to a potable stream containing 500 ppm of salt). After scale-up, the resistance may rise owing to the multi-channels and multi-layers of membranes as well as the in-series or parallel connection of devices which can cause high operating voltage and energy consumption.

In regard to the stability of the current system, a batch cycling desalination experiment was conducted in the same system by refreshing the salt feed without membrane replacement. At 0.06 mA cm^{-2}, 3000 ppm feed salt was desalted to the same level in successive cycles (Fig. S4). Moreover, there was minimal change in the ferri-/ferrocyanide UV–vis spectra after desalination (Fig. S5a). Results of this study demonstrated the excellent repeatability of the proposed system and suggest that the proposed approach would be suitable for multi-cycle desalination of brackish feed streams.

One concern related to the current design is the potential leakage of ferri-/ferrocyanide to the salt streams. As such, we tested the absorption spectra of the desalted and concentrate streams (*i.e.* streams A and B). It can be seen from Fig. S5 that the mixture of ferri-/ferrocyanide shows two overlapping peaks at 404 nm and 419 nm with a significant absorption in the UV range (Fig. S5a). However, there was negligible difference between the absorption spectra of the desalted stream (stream A) before and after the test as shown in Fig. S5b. Some transport of ferri-/ferrocyanide into the concentrate stream (stream B) over the course of the test was evident though the amount present at the conclusion of the test was relatively minor. According to the calibration in Fig. S6, the calculated concentration is the same order as the limits of detection, indicating the possible occurrence of minor leakage. It is expected that the transport into the concentrate stream could be further reduced by improvements in O-rings and/or further tightening of the metal screws. In addition, these high-quality membranes have high mechanical strength over the pH range 0–14. It can be seen from Fig. 1(a) that the cation exchange membranes directly contact with the redox couples. We therefore checked for any change in properties of the membranes after desalination. Results showed that there was no color change, suggesting minimal reaction between the redox couples and the membranes (Fig. S7). This was further confirmed by the similarity of FTIR spectra of the membranes before test and extended use (Fig. S7).

While many salts of cyanide are highly toxic, ferro- and ferricyanides are much less toxic because they tend not to release free cyanide. NFPA 704 codes of potassium ferricyanide and potassium ferrocyanide (Standard System for the Identification of the Hazards of Materials for Emergency Response) are classified as 1 (Health), 0 (Flammability), 0 (Instability–reactivity). Therefore, it is possible to conclude that ferri/ferrocyanide is stable and relatively safe under the conditions used in this work though more environment-friendly alternatives will be considered in future studies. Moreover, there was minimal change in the ferri-/ferrocyanide UV–vis spectra after desalination (Fig. S5a).

3.2. Impact of current density on desalination performance

The average salt removal rate (ASRR) is largely determined by the current density. Fig. 2a demonstrates the variations of voltage and salt content at different current densities ranging from 0.06 to 0.24 mA cm^{-2}. Voltage is displayed on the left Y axis while the salt concentrations in streams A and B are displayed on the right Y axis. The ASRR (indicated by the slopes of the concentration data in Figs. 2a and S8) increases with increase in current density, indicating that desalination occurs more rapidly at a higher current density. As shown in Fig. S8, the desalination rates are 1.24, 4.14, 6.60 and 8.86 μg cm^{-2} min^{-1} at the corresponding current densities of 0.06, 0.12, 0.18 and 0.24 mA cm^{-2}. The salt accumulation rate in stream B mirrors the removal rate in stream A with this equivalence further supporting the desalination mechanism proposed in Fig. 1a. The resistance is calculated based on the operating cell voltage and current in Fig. 2. The result is shown in Fig. S9. The value is quite low in the current system, and rises with the increased current density.

The energy consumption at various current densities is summarized

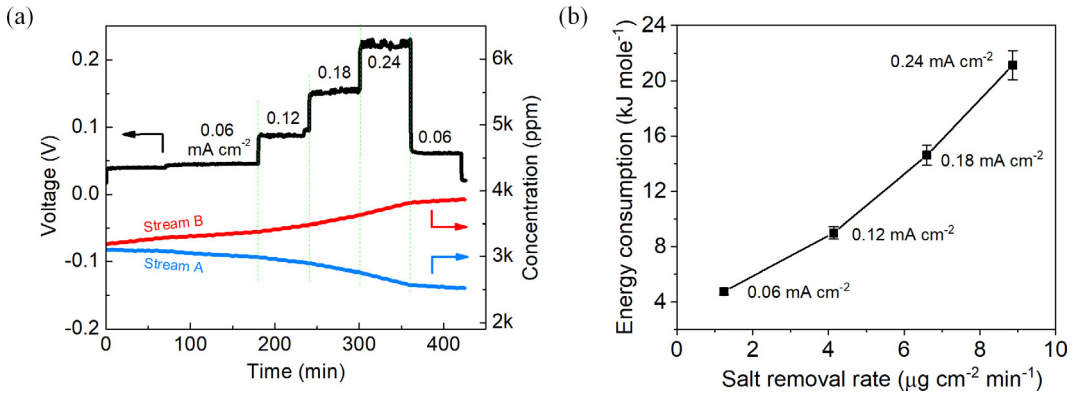

Fig. 2. (a) The redox-mediated desalination at various current densities (0.06 mA cm^{-2} for 3 h, 0.12 mA cm^{-2} for 1 h, 0.18 mA cm^{-2} for 1 h, 0.24 mA cm^{-2} for 1 h, and 0.06 mA cm^{-2} for 1 h) and (b) the curve of energy consumption ($\bar{E}$) *vs.* average salt removal rate (ASRR) at different current densities.

in Figs. 2b and S8b. At a current density of 0.06 mA cm^{-2}, the energy consumption was 4.75 kJ $mole^{-1}$. This is much lower than that exhibited by RO for which the typical operational energy consumption is ~24 kJ $mole^{-1}$ [1,35–37]. The very low energy consumption relates to the extremely low operating voltage (~50 mV) achieved as a result of the operating voltage confinement achieved via the ferri-/ferrocyanide redox reactions under the constant current condition used though it should be recognized that more energy input is required at higher current densities. For example, at current densities of 0.12, 0.18 and 0.24 mA cm^{-2}, the energy consumption rises to 9.00, 14.6, 21.1 kJ $mole^{-1}$ respectively. When a higher current density of 1.11 mA cm^{-2} (10 mA) was applied in this work, the voltage plateau became higher than 2 V, and the salt removal rate increased to 30–40 μg cm^{-2} min^{-1} with the energy efficiency compromised (Fig. S10 and Table S1). However, the energy consumption could be further reduced by increasing the surface area/sites of the current collectors. At a higher salt feed concentration (achieved via salt addition with stirring), while the salt removal rate and charge efficiency were maintained at the same level, the voltage dropped with increase in the feed concentration, resulting in lower energy consumption at higher salt feed concentration (Fig. S11). This trend is consistent with that reported in the literature [10,11,17]. The comparison of energy consumption of different desalination technologies is tabulated in Table S1. It can be noted that both CDI and battery desalination consume relatively high electrical energy [1,38–41] compared to this system. While the energy consumption may be reduced to 10.3 kJ $mole^{-1}$ with use of VCl_3/NaI in flow battery desalination [16,17], critical challenges remain in regard to the intermittent operation of the system [17]. Other more recent studies achieved 78 kJ $mole^{-1}$ energy consumption using the metal-free 4-hydroxy-2,2,6,6-tetramethylpiperidine 1-oxyl as redox mediator [27], and 96.8 kJ $mole^{-1}$ using battery electrode deionization [10,11]. In comparison with the other recent published work in which ferri-/ferrocyanide is used either as an electrochemical analysis tool to probe the possibility of capacitive desalination applications [42] or as redox couple to remove salt [28], the recycling of ferri-/ferrocyanide in this study resulted in more efficient salt removal; that is, even at the much higher desalination rate achieved here (~40 μg cm^{-2} min^{-1} compared to 5–25 μg cm^{-2} min^{-1}), the energy costs were comparable (Table S1)

3.3. Effect of concentration of the ferri-/ferrocyanide redox couple

The concentration of the ferri-/ferrocyanide redox couple can also affect the desalination performance. Figs. 3a and S12 show the voltage change during desalination under a range of concentrations of the ferri-/ferrocyanide redox couple at various current densities. At a higher mediator concentration, there should exist more contact and reaction opportunities between the current collectors and the redox mediators resulting in a rapid rate of electron transfer and a low voltage plateau. In 10 mM/10 mM ferri-/ferrocyanide, the average $\bar{E}$ can be reduced to 2.14 kJ $mole^{-1}$ during the first three hours, which is the lowest value currently reported (when the desalination process was driven by a 0.06 mA cm^{-2} constant current density). As shown in Figs. 3b and S12, there is significant difference in desalination performance between the desalination system using 1 mM/1 mM ferri-/ferrocyanide and that using 2 mM/2 mM ferri-/ferrocyanide. This is likely related to the high over-potential of the redox reaction in the presence of insufficient ferricyanide/ferrocyanide (See Section 3.4). However, the improvement became marginal when the concentrations exceeded 2 mM. Comparatively high concentrations might saturate the reaction sites, resulting in the availability of surface sites (and/or current density) becoming rate limiting. A comparable test was therefore conducted at a much higher current density (1.11 mA cm^{-2}). The results demonstrated that the desalination performance could be slightly improved on increasing the ferricyanide/ferrocyanide concentration from 2 mM/2 mM to 50 mM/50 mM (Fig. S13). However, the improvement was marginal due to the saturation of reaction sites in the 2 mM/2 mM ferricyanide/ferrocyanide system.

Alternatively, this can be expressed by noting that ASRR and $\bar{E}$ largely depend on the ferri-/ferrocyanide concentration (and current density). Furthermore, high charge efficiency can be obtained at high current density and high ferri-/ferrocyanide concentrations (Fig. S14). Based on the desalination mechanism in Fig. 1a, most of the input electrons should be involved in salt removal from stream A to stream B as a result of the high charge efficiency of the system. It can be seen from Fig. S15 that the salt removal rate in stream A is, experimentally, equal to the salt accumulation rate in stream B.

3.4. The mechanism of low energy consumption

The desalination process was conducted at a constant current with high charge efficiency. Hence, the energy consumption is only affected by the operating voltage plateau. As such, it would seem reasonable to conclude that the overpotential is likely to be the key factor influencing the energy consumption. The overpotential behavior of the ferri-/ferrocyanide redox couple at the various concentrations was investigated by linear sweep voltammetry (LSV) using a rotating disk electrode. The results are shown in Fig. S16 where LSV curves are seen to be symmetrical with the redox limiting currents extracted at both high and low potentials in the 1 mM/1 mM, 2 mM/2 mM, 5 mM/5 mM, and 10 mM/10 mM ferri-/ferrocyanide solutions. The reciprocal of the limiting current *vs.* the reciprocal of the square root of the rotation rates calculated by the Koutecky-Levich equation for ferricianide and ferrocyanide at different concentrations are linear plots as demonstrated in Fig. S17 and Table S2. The absolute values of the slope increase with an increase in the concentration of ferri-/ferrocyanide. The fitted Tafel plots of overpotential *vs.* $\log_{10}(|i_K|)$ are provided in Fig. 4(a) where the

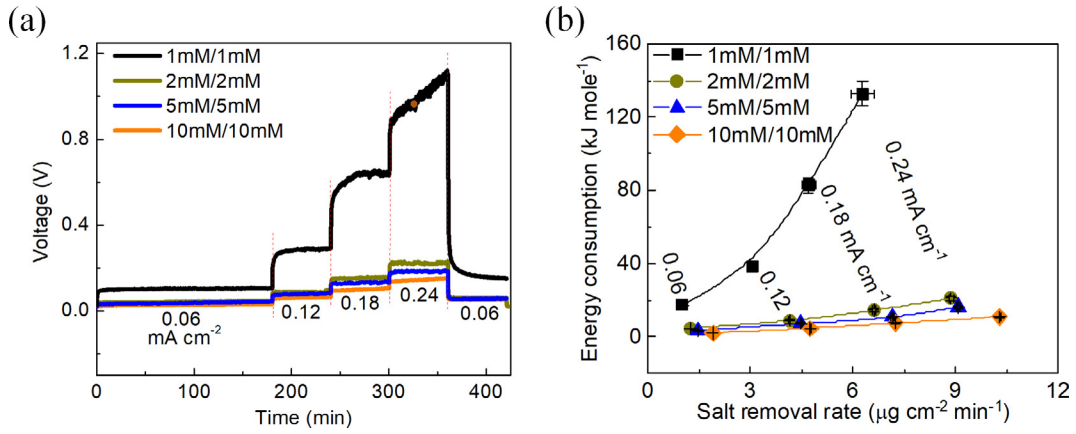

Fig. 3. The concentration effects of ferri-/ferrocyanide redox mediators at various current densities, *i.e.* 1 mM/1 mM ferri-/ferrocyanide (black), 2 mM/2 mM ferri-/ferrocyanide (dark yellow), 5 mM/5 mM ferri-/ferrocyanide (blue) and 10 mM/10 mM ferri-/ferrocyanide (orange). (a) The operating voltages as a function of time at various ferri-/ferrocyanide concentrations. (b) Energy consumption ($\bar{E}$) *vs.* average salt removal rate (ASRR) at various ferri-/ferrocyanide concentrations and current densities. (For interpretation of the references to color in this figure legend, the reader is referred to the web version of this article.)

i_K values are the intercept currents of the Y axis of Fig. S17 derived from the corresponding Koutecky-Levich plots (Eq. (1)). At the same overpotential value, the logarithm of the current is higher at higher concentrations of the ferri-/ferrocyanide redox couples, which indicates a higher current as shown in Fig. 4a. Similarly, the lowest overpotential value can be obtained at the highest concentration under the same logarithm of current as displayed in Fig. 4b. In the current tests, 10 mM/10 mM ferri-/ferrocyanide solutions were chosen as the highest concentration, and it possesses the lowest overpotential, which is consistent with the lowest voltage plateau (Fig. 3a). The high concentration redox species provide more reaction opportunities between electrolytes and electrodes and fast kinetic reaction under the same condition.

Results of this study demonstrate that the voltage plateau during desalination can be influenced by the composition of the redox couple. Fig. S18 shows that the redox couple has better electrochemical activity compared to the individual mediators at the same concentration, which is directly related to the energy consumption that is given in Fig. S19. For example, 2 mM/2 mM ferri-/ferrocyanide results in a ~0.05 V potential plateau. However, the voltage plateau of as-prepared 4 mM ferricyanide is stable at ~0.5 V. This may be due to the slow oxidation reaction from the insufficient ferrocyanide with this resulting in a sluggish kinetic process. The LSV results of the three samples are provided in Fig. S20. The fitted Tafel plot of overpotential *vs.* $\log_{10}(|i_K|)$ in Fig. 5a can be extracted from the Koutecky–Levich plots in Fig. S21 and Table S3. It is found that the overpotential in ferri-/ferrocyanide is much lower in mixed ferri-/ferrocyanide solution than that of pure ferricyanide or ferrocyanide solutions at the same current as shown in Fig. 5b, which largely explains the higher energy consumption in pure ferricyanide or ferrocyanide solutions. The low energy consumption is likely a result of the synergistic effect of sufficient simultaneous ferrocyanide oxidation and ferricyanide reduction in the flow electrolyte streams, resulting in smooth electron transfer between cathode and anode in the outer circuit, even at the low operating voltage used.

4. Conclusion

In this study, a very low energy continuous desalination approach has been developed using the ferri-/ferrocyanide redox couple. The cathode in the flowing ferri-/ferrocyanide solution will accept the cation from stream A and then release this cation to stream B on the anode side, with no cation accumulation or pH change in the cathode chamber. Due to the synergistic effects of the electron transfer resulting from ferrocyanide oxidation at anode and ferricyanide reduction at cathode at the same time (1:1 M ratio of ferrocyanide and ferricyanide in the flowing electrolyte streams), the operating potential can be maintained at ~100 mV at a constant current density of 0.06 mA cm^{-2}, resulting in an average energy consumption as low as 8.34–7.96 kJ $mole^{-1}$ with salt feed desalinated from 3000 to

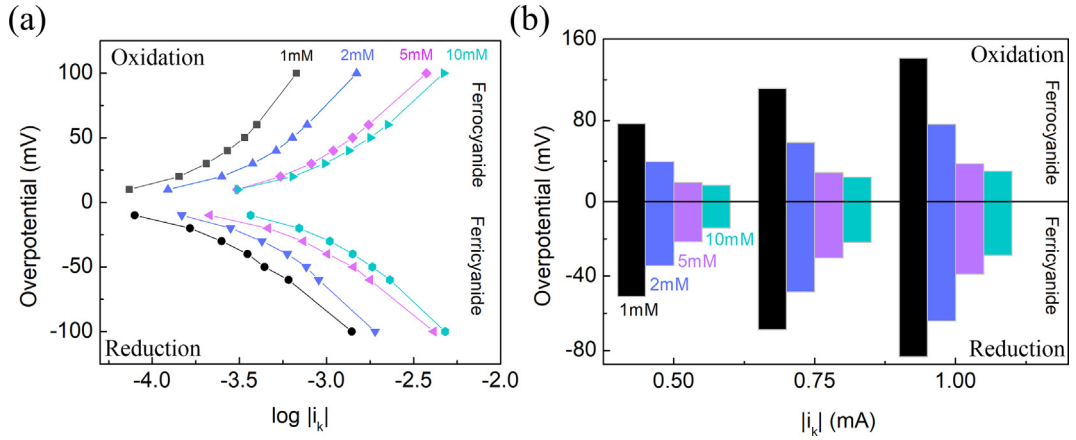

Fig. 4. The overpotential of ferri-/ferrocyanide redox couples at various concentrations and current densities. (a) The fitted Tafel plot of overpotentials *vs.* $\log_{10}(|i_K|)$ and (b) the overpotential comparison at 0.5 mA, 0.75 mA, and 1 mA current for 1 mM/1 mM, 2 mM/2 mM, 5 mM/5 mM and 10 mM/10 mM ferri-/ferrocyanide redox couples. $\log_{10}(|i_K|)$ values were retrieved from the Koutecky-Levich plots in Fig. S17 and Table S2. The three currents of 0.5 mA, 0.75 mA, and 1 mA were retrieved from Fig. 4a as examples (log 0.5 mA = −3.301, log 0.75 mA = −3.125, log 1 mA = −3).

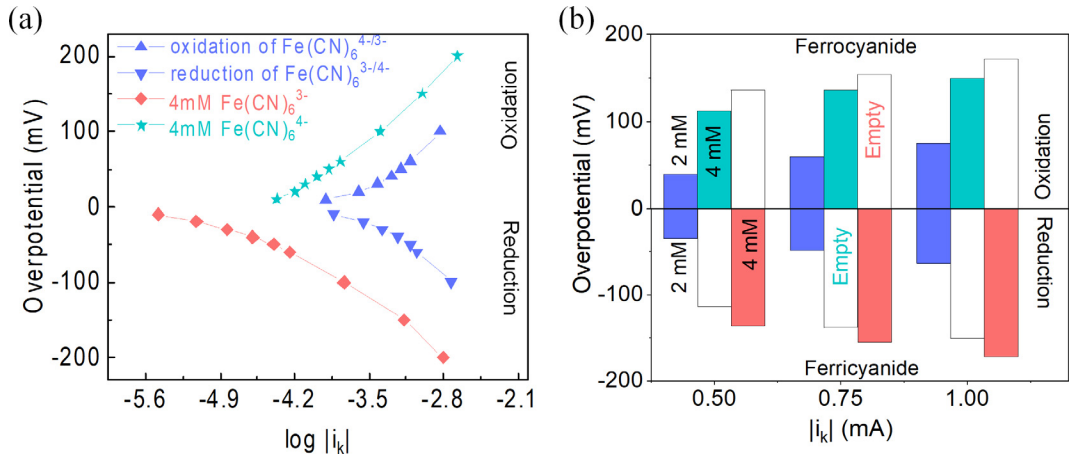

Fig. 5. The overpotential comparison of 2 mM/2 mM ferri-/ferrocyanide, pure 4 mM ferrocyanide, and pure 4 mM ferricyanide. (a) The fitted Tafel plot of overpotentials *vs.* $\log_{10}(|i_K|)$ and (b) the overpotential comparison at 0.5, 0.75 and 1.0 mA. $\log_{10}(i_K)$ values were derived from the Koutecky–Levich plots in Fig. S21 and Table S3. The three currents of 0.5, 0.75 and 1 mA were retrieved from Fig. 5a as examples (log 0.5 mA = −3.301, log 0.75 mA = −3.125, log 1 mA = −3).

150–500 ppm. When the concentration of ferri-/ferrocyanide is increased to 10 mM/10 mM, an even lower energy consumption of 2.14 kJ mole^{-1} was achieved during the first three hours of operation. The extremely low energy consumption can be attributed to the rapid rate of electron transfer between the ferri-/ferrocyanide redox couple with this property resulting in very low overpotentials (as confirmed here by LSV measurement).

Overall, this study has demonstrated a promising route for the continuous desalination of brackish feed waters at ultra-low energy. While we have focused in the current study on the desalination of a brackish feed water, salt removal from more saline feed streams (such as seawater) may be possible. In addition to the need for further optimisation of operating parameters, selection of cheaper and safer redox compounds, evaluation of the matrix effects and productivity scale-up, further consideration should be given to the management of the concentrate, especially in inland areas where the discharge of the brine stream could be problematic. Nevertheless, with regard to the negligible concentration of ferri-/ferrocyanide in the brine, the current system could be integrated with other zero-discharge technologies (e.g. solar evaporation) to minimize any secondary pollution. Nevertheless, in regard to the negligible ferri-/ferrocyanide in the brine, the current system could be integrated with other zero-discharge technologies (e.g. solar evaporation) to minimize the secondary pollution. These efforts are oriented towards the practical application of the proposed system such that continuous desalination for freshwater production can be achieved in a facile manner.

Declaration of Competing Interest

The authors declare that they have no known competing financial interests or personal relationships that could have appeared to influence the work reported in this paper.

Acknowledgements

This project was supported by South China Normal University, SCNU Outstanding Young Scholar Project (8S0256), the Scientific and Technological Plan of Guangdong Province (2018A050506078). F. Chen acknowledges the Pearl River Talent Program (2019QN01L951)

Appendix A. Supplementary data

Supplementary data to this article can be found online at https://doi.org/10.1016/j.cej.2020.126111.

References

[1] R. Zhao, S. Porada, P.M. Biesheuvel, A. van der Wal, Energy consumption in membrane capacitive deionization for different water recoveries and flow rates, and comparison with reverse osmosis, Desalination 330 (2013) 35–41.
[2] Y. Wang, I. Vázquez-Rodríguez, C. Santos, E. García-Quismondo, J. Palma, M.A. Anderson, J.J. Lado, Graphite felt 3D framework composites as an easy to scale capacitive deionization electrode for brackish water desalination, Chem. Eng. J. 392 (2020) 123698.
[3] K. Tang, Y.-H. Kim, J. Chang, R.T. Mayes, J. Gabitto, S. Yiacoumi, C. Tsouris, Seawater desalination by over-potential membrane capacitive deionization: opportunities and hurdles, Chem. Eng. J. 357 (2019) 103–111.
[4] M. Pasta, C.D. Wessells, Y. Cui, F. La Mantia, A desalination battery, Nano Lett. 12 (2012) 839–843.
[5] F. La Mantia, M. Pasta, H.D. Deshazer, B.E. Logan, Y. Cui, Batteries for efficient energy extraction from a water salinity difference, Nano Lett. 11 (2011) 1810–1813.
[6] X. Xu, A.E. Allah, C. Wang, H. Tan, A.A. Farghali, M.H. Khedr, V. Malgras, T. Yang, Y. Yamauchi, Capacitive deionization using nitrogen-doped mesostructured carbons for highly efficient brackish water desalination, Chem. Eng. J. 362 (2019) 887–896.
[7] R.L. Zornitta, L.A.M. Ruotolo, Simultaneous analysis of electrosorption capacity and kinetics for CDI desalination using different electrode configurations, Chem. Eng. J. 332 (2018) 33–41.
[8] J. Ma, D. He, W. Tang, P. Kovalsky, C. He, C. Zhang, T.D. Waite, Development of redox-active flow electrodes for high-performance capacitive deionization, Environ. Sci. Technol. 50 (2016) 13495–13501.
[9] B. Han, G. Cheng, Y. Wang, X. Wang, Structure and functionality design of novel carbon and faradaic electrode materials for high-performance capacitive deionization, Chem. Eng. J. 360 (2019) 364–384.
[10] F. Chen, Y. Huang, L. Guo, L. Sun, Y. Wang, H.Y. Yang, Dual-ions electrochemical deionization: a desalination generator, Energy Environ. Sci. 10 (2017) 2081–2089.
[11] F. Chen, Y. Huang, L. Guo, M. Ding, H.Y. Yang, A dual-ion electrochemistry deionization system based on AgCl-Na0.44MnO2 electrodes, Nanoscale 9 (2017) 10101–10108.
[12] D.-H. Nam, K.-S. Choi, Bismuth as a new chloride-storage electrode enabling the construction of a practical high capacity desalination battery, J. Am. Chem. Soc. 139 (2017) 11055–11063.
[13] J. Lee, S. Kim, J. Yoon, Rocking chair desalination battery based on Prussian blue electrodes, ACS Omega 2 (2017) 1653–1659.
[14] S. Porada, A. Shrivastava, P. Bukowska, P.M. Biesheuvel, K.C. Smith, Nickel hexacyanoferrate electrodes for continuous cation intercalation desalination of brackish water, Electrochim. Acta 255 (2017) 369–378.
[15] T. Kim, C.A. Gorski, B.E. Logan, Low energy desalination using battery electrode deionization, Environ. Sci. Technol. Lett. 4 (2017) 444–449.
[16] D. Desai, E.S. Beh, S. Sahu, V. Vedharathinam, Q. van Overmeere, C.F. de Lannoy, A.P. Jose, A.R. Völkel, J.B. Rivest, Electrochemical desalination of seawater and hypersaline brines with coupled electricity storage, ACS Energy Lett. 3 (2018) 375–379.
[17] X. Hou, Q. Liang, X. Hu, Y. Zhou, Q. Ru, F. Chen, S. Hu, Coupling desalination and energy storage with redox flow electrodes, Nanoscale 10 (2018) 12308–12314.
[18] F. Chen, Y. Huang, D. Kong, M. Ding, S. Huang, H.Y. Yang, NaTi2(PO4)3-Ag electrodes based desalination battery and energy recovery, FlatChem 8 (2018) 9–16.
[19] M.E. Suss, V. Presser, Water desalination with energy storage electrode materials, Joule 2 (2018) 10–15.
[20] S. Liu, K.C. Smith, Quantifying the trade-offs between energy consumption and salt removal rate in membrane-free cation intercalation desalination, Electrochim. Acta 271 (2018) 652–665.
[21] P. Srimuk, J. Lee, S. Fleischmann, S. Choudhury, N. Jäckel, M. Zeiger, C. Kim,

M. Aslan, V. Presser, Faradaic deionization of brackish and sea water via pseudo-capacitive cation and anion intercalation into few-layered molybdenum disulfide, J. Mater. Chem. A 5 (2017) 15640–15649.
[22] C. Zhang, D. He, J. Ma, W. Tang, T.D. Waite, Faradaic reactions in capacitive deionization (CDI) - problems and possibilities: a review, Water Res. 128 (2018) 314–330.
[23] Y. Huang, F. Chen, L. Guo, J. Zhang, T. Chen, H.Y. Yang, Low energy consumption dual-ion electrochemical deionization system using NaTi2 (PO4) 3-AgNPs electrodes, Desalination 451 (2019) 241–247.
[24] J. Veerman, M. Saakes, S.J. Metz, G.J. Harmsen, Reverse electrodialysis: evaluation of suitable electrode systems, J. Appl. Electrochem. 40 (2010) 1461–1474.
[25] O. Scialdone, C. Guarisco, S. Grispo, A.D. Angelo, A. Galia, Investigation of electrode material – redox couple systems for reverse electrodialysis processes. Part I: iron redox couples, J. Electroanal. Chem. 681 (2012) 66–75.
[26] M.E. Suss, S. Porada, X. Sun, P.M. Biesheuvel, J. Yoon, V. Presser, Water desalination via capacitive deionization: what is it and what can we expect from it? Energy Environ. Sci. 8 (2015) 2296–2319.
[27] J. Wang, Q. Zhang, F. Chen, X. Hou, Z. Tang, Y. Shi, P. Liang, D.Y.W. Yu, Q. He, L.-J. Li, Continuous desalination with a metal-free redox-mediator, J. Mater. Chem. A 7 (2019) 13941–13947.
[28] N. Kim, S.P. Hong, J. Lee, C. Kim, J. Yoon, High-desalination performance via redox couple reaction in the multichannel capacitive deionization system, ACS Sustain. Chem. Eng. 7 (2019) 16182–16189.
[29] E.S. Beh, M.A. Benedict, D. Desai, J.B. Rivest, A redox-shuttled electrochemical method for energy-efficient separation of salt from water, ACS Sustain. Chem. Eng. 7 (2019) 13411–13417.
[30] J. Ma, C. He, D. He, C. Zhang, T.D. Waite, Analysis of capacitive and electrodialytic contributions to water desalination by flow-electrode CDI, Water Res. 144 (2018) 296–303.
[31] C. He, J. Ma, C. Zhang, J. Song, T.D. Waite, Short-circuited closed-cycle operation of flow-electrode CDI for brackish water softening, Environ. Sci. Technol. 52 (2018) 9350–9360.
[32] S. Al-Amshawee, M.Y.B.M. Yunus, A.A.M. Azoddein, D.G. Hassell, I.H. Dakhil, H.A. Hasan, Electrodialysis desalination for water and wastewater: a review, Chem. Eng. J. 380 (2020) 122231.
[33] Z. Song, S. Garg, J. Ma, T.D. Waite, Modified double potential step chronoamperometry (DPSC) method for As(III) electro-oxidation and concomitant As(V) adsorption from groundwaters, Environ. Sci. Technol. 53 (2019) 9715–9724.
[34] Y. Cho, K.S. Lee, S. Yang, J. Choi, H.-R. Park, D.K. Kim, A novel three-dimensional desalination system utilizing honeycomb-shaped lattice structures for flow-electrode capacitive deionization, Energy Environ. Sci. 10 (2017) 1746–1750.
[35] S. Choi, B. Chang, J.H. Kang, M.S. Diallo, J.W. Choi, Energy-efficient hybrid FCDI-NF desalination process with tunable salt rejection and high water recovery, J. Membr. Sci. 541 (2017) 580–586.
[36] M. Elimelech, W.A. Phillip, The future of seawater desalination: energy, technology, and the environment, Science 333 (2011) 712–717.
[37] S. Lin, M. Elimelech, Staged reverse osmosis operation: configurations, energy efficiency, and application potential, Desalination 366 (2015) 9–14.
[38] J.H. Choi, D.J. Yoon, A stable operation method for membrane capacitive deionization systems without electrode reactions at high cell potentials, Water Res. 157 (2019) 167–174.
[39] R. Zhao, P.M. Biesheuvel, A. van der Wal, Energy consumption and constant current operation in membrane capacitive deionization, Energy Environ. Sci. 5 (2012) 9520–9527.
[40] C. Kim, P. Srimuk, J. Lee, M. Aslan, V. Presser, Semi-continuous capacitive deionization using multi-channel flow stream and ion exchange membranes, Desalination 425 (2018) 104–110.
[41] C. Kim, P. Srimuk, J. Lee, V. Presser, Enhanced desalination via cell voltage extension of membrane capacitive deionization using an aqueous/organic bi-electrolyte, Desalination 443 (2018) 56–61.
[42] A. Sene, B. Daffos, P.-L. Taberna, P. Simon, Characterization of the mass transfer fluxes in a capacitive desalination cell by using FeIII(CN)63 − /FeII(CN)64 − redox couple as an electrochemical probe, J. Electroanal. Chem. 842 (2019) 127–132.